

# Fluorinated Solvent-Coupled Anion-Derived Interphase to Stabilize Silicon Microparticle Anodes for High-Energy-Density Batteries

Yan Liu, Yutong Huang, Xin Xu, Yang Liu, Jianghong Yang, Jiawei Lai, Junkai Shi, Shuxian Wang, Weizhen Fan,\* Yue-Peng Cai, Ya-Qian Lan,\* and Qifeng Zheng\*

Si microparticle (SiMP) anodes feature much lower production cost and higher tap density compared to their nanosized counterparts, which hold great promise for high-energy-density lithium-ion batteries, yet they suffer from unavoidable particle pulverization during repeated cycling, thus making their practical application extremely challenging. Herein, a non-flammable localized high-concentration electrolyte (LHCE) is rationally formulated using a fluorinated solvent, 2,2,2-trifluoroethyl methyl carbonate (FEMC), to induce fluorinated solvent-coupled anion-derived interfacial chemistry. Unlike other LHCEs, the FEMC-based LHCE is demonstrated to build a highly robust and stable F-rich inorganic–organic bilayer solid–electrolyte interphase on SiMP anode, which endows stable cycling of SiMP anode ( $\approx 3.4 \text{ mAh cm}^{-2}$ ) with an ultrahigh Coulombic efficiency of  $\approx 99.7\%$ . Coupled with its high anodic stability, the FEMC-based LHCE endows unprecedented cycling stability for high-energy-density batteries containing high-capacity SiMP anodes with Ni-rich  $\text{LiNi}_8\text{Mn}_1\text{Co}_1\text{O}_2$  or 5 V-class  $\text{LiNi}_{0.5}\text{Mn}_{1.5}\text{O}_4$  cathodes. Remarkably, a 1.0 Ah-level SiMP|| $\text{LiNi}_8\text{Mn}_1\text{Co}_1\text{O}_2$  pouch-cell stably operates for more than 200 cycles, representing the pioneering report in pouch cells containing SiMP anodes.

with a low operating potential of  $\approx 0.2 \text{ V}$  vs  $\text{Li/Li}^+$ ) and high-voltage high-capacity Ni-rich  $\text{LiNi}_8\text{Mn}_1\text{Co}_1\text{O}_2$  (NMC811) layered cathodes ( $>200 \text{ mAh g}^{-1}$  at a upper cut-off voltage of  $\geq 4.4 \text{ V}$  vs  $\text{Li/Li}^+$ ) or high-voltage spinel  $\text{LiNi}_{0.5}\text{Mn}_{1.5}\text{O}_4$  (LNMO) cathodes ( $147 \text{ mAh g}^{-1}$  with an operating potential of  $4.7 \text{ V}$  vs  $\text{Li/Li}^+$ ) has been regarded as the prime choices.<sup>[3,4]</sup> However, both Si anode and NMC811/LNMO cathodes suffer from severe structural instabilities and electrode–electrolyte parasitic reactions that quickly deteriorates the battery performance.

In addition to its ultra-high theoretical specific capacity, Si is also the second most abundant element in the earth's crust and being environmental friendly.<sup>[5]</sup> Especially, Si microparticle (SiMP) is featured with low production cost and high tap density,<sup>[6]</sup> which makes SiMP a much more promising anode materials than Si nanoparticle (SiNP) for industrial applications. Nevertheless, SiMP anode encounters serious structural pulverization owing to its large size as well as vast volume changes ( $>300\%$ ) upon lithiation/delithiation, which leads to

excessive growth of the solid–electrolyte interphase (SEI), loss of electrical contact, and low Coulombic efficiency (CE).<sup>[3,7]</sup> Therefore, the stable cycling of SiMP anode is extremely challenging. Encapsulating the SiMP with various carbon materials has been demonstrated to mitigate the pulverization, whereas the complex fabrication and compromised capacity (generally below  $2000 \text{ mAh g}^{-1}$ ) has hindered their practical applications.<sup>[8–10]</sup> Robust binders with super-elastic and self-healing properties can cushion the volume expansion and keep the pulverized SiMP coalesced.<sup>[11–13]</sup> Great improvement in cycling stability has been achieved in half-cell tests with large lithium excess, while most full-cells are limited to 100 cycles except for those with prelithiation step,<sup>[10,14]</sup> which adds significant cost to the batteries.

Engineering electrolyte formulations to tune the SEI chemistry has also been widely investigated to improve the cycability of the Si-based anodes.<sup>[15,16]</sup> Electrolyte additives,<sup>[17]</sup> such as fluoroethylene carbonate (FEC) has been commonly employed because it can contribute to a mechanically stable LiF-containing organic–inorganic hybrid SEI.<sup>[18]</sup> In addition, other fluorine-donating additives such as trifluoropropylene

## 1. Introduction

To meet the ever-increasing demands of portable electronics, electrical vehicles, and stationary energy storage systems, developing rechargeable lithium-ion batteries (LiBs) with higher energy density and lower cost is of vital importance.<sup>[1,2]</sup> As the energy density is proportional to the capacity and working voltage of a LiB, the combination of high-capacity Si anodes ( $3579 \text{ mAh g}^{-1}$

Y. Liu, Y. Huang, X. Xu, Y. Liu, J. Yang, J. Lai, J. Shi, S. Wang, W. Fan, Y.-P. Cai, Y.-Q. Lan, Q. Zheng  
School of Chemistry  
Guangzhou Key Laboratory of Materials for Energy Conversion and Storage  
South China Normal University  
Guangzhou, Guangdong 510006, China  
E-mail: 2022010170@m.scnu.edu.cn; yqlan@m.scnu.edu.cn; qifeng.zheng@m.scnu.edu.cn

The ORCID identification number(s) for the author(s) of this article can be found under <https://doi.org/10.1002/adfm.202303667>

DOI: 10.1002/adfm.202303667

carbonate,<sup>[19]</sup> tris(pentafluorophenyl)borane,<sup>[20]</sup> and lithium difluoro(oxalato)borate<sup>[21]</sup> have also been demonstrated to build F-rich SEIs on Si-based anodes. Furthermore, vinylene carbonate (VC) and its derivatives were also studied to generate poly(VC) SEI species.<sup>[22,23]</sup> Although improved cycling performance was achieved for various SiNP-based anodes, the effectiveness of these additives was brutally deteriorated for SiMP anodes.

Tailoring inorganic SEI components with high interfacial energy and excellent mechanical strength paves a new direction to stabilize the SiMP anodes, which can be realized by increasing the concentration of lithium salts (i.e., high-concentration electrolytes (HCEs)).<sup>[24]</sup> The HCEs are able to extensively recruit anions into the Li<sup>+</sup> inner solvation sheath while reduce the solvent coordination, leading to anion-derived inorganic-rich SEIs. For that, Chen et al. formulated a 2.0 M lithium hexafluorophosphate (LiPF<sub>6</sub>) in tetrahydrofuran/2-methyltetrahydrofuran ether solvents, in which the PF<sub>6</sub><sup>-</sup> anion is prior reduced to generate a high-purity LiF inner SEI layer and the ether solvents is subsequently reduced to generate an organic outer SEI layer, yielding a high-modulus LiF-organic bilayer SEI that sustains the stable cycling of SiMP anode with high CE.<sup>[25]</sup> However, poor oxidative stability and high flammability nature of the ether solvents hinder its application with high-voltage cathodes and raises potential safety incidents.

To solve the high viscosity, poor wettability, and high cost shortcomings associated with HCEs, Xu and Zhang's group proposed the concept of localized HCEs (LHCEs)<sup>[26,27]</sup> in which the anion-rich solvation structure can be locally maintained via diluting the HCEs with non-solvating solvent. Recently, the LHCEs were explored to tolerate the volume changes of Si-based anodes by generating an inorganic-rich SEI with high mechanical strength.<sup>[28–30]</sup> Nevertheless, their availabilities were only proved in nanosized Si or Si/graphite anodes, which is probably ascribed to the fact that solely rigid inorganic SEIs is not sufficient to withstand the huge volume change of micro-sized Si anode. For SiMP anode, an ideal SEI should consist of a high-modulus inorganic inner layer to accommodate the plastic deformation of SiMP, and a dense, strong yet pliable organic outer layer that acts as buffer layer to provide support for the inorganic inner layer as well as to prevent parasitic reaction with electrolytes. Over the past decade, extensive research has been focused on constructing inorganic SEI components, while little attention has been paid to this organic outer layer.

Herein, we rationally formulate a LHCE consists of 2.0 M lithium bis(fluorosulfonyl)imide (LiFSI) dissolved in a mixture solvent of 2,2,2-trifluoroethyl methyl carbonate (FEMC) solvent and 1H,1H,5H-octafluoroamyl-1,1,2,2-tetrafluoroether (OTE) diluent (FEMC:OTE = 1:1 by vol., here 2.0 M stands for 2.0 mol salt dissolved in 1 L solvent). The FEMC was selected as a solvent owing to the following several merits: 1) the fluorine moiety could lower the highest occupied molecular orbital (HOMO) of the FEMC, thereby increasing its oxidation stability and making the electrolyte compatible with high-voltage cathodes; 2) the fluorine moiety could also weaken the solvating ability of the FEMC solvent, further promoting the Li<sup>+</sup>-FSI<sup>-</sup> pairing, which may lead to a high-purity inorganic inner SEI layer; 3) most importantly, the subsequent reduction of FEMC solvent with CF<sub>3</sub>-moiety would contribute to a F-rich organic outer SEI components, thus is expected to yield a highly robust and stable

F-rich inorganic-organic bilayer SEI. The solvation structure and interfacial properties of this FEMC-based LHCE was carefully investigated from both experimental and theoretical aspects. Moreover, on the application of this FEMC-based LHCE, the stable cycling of Li||SiMP half-cells, high-voltage high-energy-density SiMP||NMC811 and SiMP||LNMO coin, and pouch full-cells (Ah level) was systematically examined.

## 2. Results and Discussion

### 2.1. Design Principle and Solvation Structure of the Electrolytes

As shown in **Figure 1a**, the carbonate solvent, such as ethyl methyl carbonate (EMC), has been commonly employed in the battery electrolytes. For the conventional EMC-based regular concentration electrolyte ( $\approx 1$  M, denoted as EMC-RCE), the Li<sup>+</sup> is strongly coordinated with solvent to form a solvent-dominated solvation structure, leading to a solvent-derived organic-dominated SEI, which is porous with low modulus and low interfacial energy that cannot tolerate the vast volume change of the SiMP anode and usually fails within a few cycles. To improve the mechanical strength of the SEI, the concentration of the lithium salts was increased (typically  $> 3.0$  M, denoted as EMC-HCE) and the primary solvation sheath becomes dominating by anions, contributing to an anion-derived inorganic-dominated SEI, which is rigid with high-modulus but can be fragile that is not sufficient to withstand the vast volume change of the SiMP anode upon repeated cycling. In addition, the HCEs suffer from high viscosity and high cost, therefore non-solvating solvent was introduced to dilute the high concentration while maintaining locally anion-rich solvation structure (denoted as EMC-LHCE).

Aiming to build a dense and strong buffer layer in addition to the rigid inorganic inner layer, the conventional EMC solvent was replaced with a fluorinated FEMC solvent (**Figure 1b**). Owing to its lowered HOMO and LUMO (i.e., lowest unoccupied molecular orbital) of FEMC, the resulting FEMC-RCE is expected to possess high oxidation stability and generates a F-rich organic-dominated SEI with improved interfacial energy that is strong yet pliable. After increasing the concentration of the lithium salt and then diluted with non-solvating solvent, the rationalized FEMC-LHCE combines the advantages of anion- and fluorinated solvent-derived interfacial chemistry, which would lead to a highly robust and stable F-rich inorganic-organic bilayer SEI that can accommodate the vast volume change of the SiMP anodes.

The solvation structure of the electrolytes, namely FEMC-RCE (i.e., 1.0 M LiFSI in FEMC), FEMC-HCE (i.e., 4.0 M LiFSI in FEMC), FEMC-LHCE (i.e., 2.0 M LiFSI in FEMC/OTE), and EMC-LHCE (i.e., 2.0 M LiFSI in EMC/OTE), was first investigated by the molecular dynamics (MD) simulations in **Figures S1 and S2**, Supporting Information. To qualify the local environment around the Li<sup>+</sup> in the electrolyte solutions, the radial distribution of oxygen from both solvent and anion was calculated from MD simulations. As shown in **Figure 2a**, for FEMC-RCE, the average coordination number of Li<sup>+</sup> with FEMC oxygen (termed as O-FEMC) and FSI<sup>-</sup> oxygen (termed as O-FSI<sup>-</sup>) in the first solvation sheath (i.e., within 3.5 Å) was calculated to be Li<sup>+</sup>(O-FEMC)<sub>2.6</sub>(O-FSI<sup>-</sup>)<sub>1.8</sub> with a low FSI<sup>-</sup>/FEMC ratio of  $\approx 0.7$  (**Figure S3**, Supporting Information), indicating a FEMC solvent-dominated

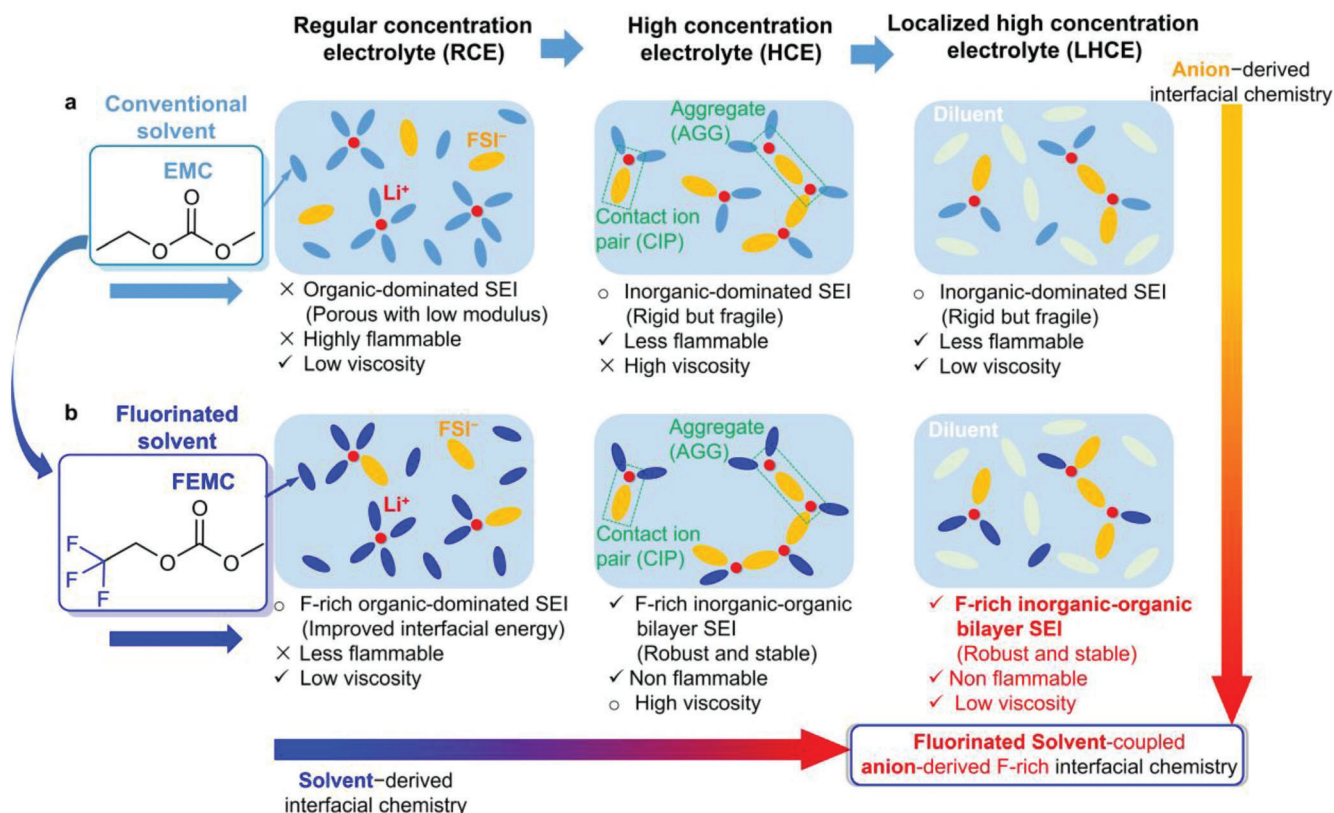


**Figure 1.** Electrolyte design principle for SiMP. Schematic illustration of solution structures and their merits of the a) conventional EMC-based electrolytes and b) fluorinated FEMC-based electrolytes. EMC is a conventional electrolyte solvent that strongly coordinates with  $\text{Li}^+$  in EMC-RCE, which tends to generate a solvent-derived organic-dominated SEI that is porous with low modulus. Increasing the salt concentration changes the electrolyte structure from solvent-rich to anion-rich solvation in EMC-HCE, and the anion-rich solvation structure can be well maintained in EMC-LHCE while lowering solution viscosity, generating an inorganic-dominated SEI that is rigid with high-modulus but can be fragile. Fluorinated FEMC solvent with lowered HOMO and LUMO is expected to possess high oxidation stability and contributes a F-rich organic SEI components that is strong yet pliable. Thus replacing the EMC with FEMC, the resulting FEMC-LHCE would generate a highly robust and stable F-rich inorganic–organic bilayer SEI that can accommodate the vast volume change of the SiMP anode.

solvation structure. After increasing the LiFSI concentration in FEMC-HCE, a large portion of  $\text{FSI}^-$  anions were drawn into the inner solvation sheath and the average coordination environment changes to  $\text{Li}^+(\text{O-FEMC})_{1.8}(\text{O-FSI}^-)_{2.6}$  with a high  $\text{FSI}^-/\text{FEMC}$  ratio of  $\approx 1.4$  (Figure 2b and Figure S3, Supporting Information). After diluting the FEMC-HCE with a non-solvating OTE solvent, the resulting FEMC-LHCE exhibits an average coordination environment of  $\text{Li}^+(\text{O-FEMC})_{1.6}(\text{O-FSI}^-)_{2.8}$  with a high  $\text{FSI}^-/\text{FEMC}$  ratio of  $\approx 1.8$  (Figure 2c and Figure S3, Supporting Information), suggesting that the addition of OTE dilution could further reduce the  $\text{Li}^+-\text{FEMC}$  coordination and boost  $\text{Li}^+-\text{FSI}^-$  pairing, which may lead to a high-purity inorganic inner SEI layer with high-modulus. While for the conventional EMC solvent (i.e., non-fluorinated), the EMC-LHCE displays an average coordination environment of  $\text{Li}^+(\text{O-EMC})_{1.9}(\text{O-FSI}^-)_{2.5}$  with a  $\text{FSI}^-/\text{FEMC}$  ratio of  $\approx 1.3$  (Figures S2 and S3, Supporting Information), which is lower than that of FEMC-LHCE (i.e.,  $\approx 1.8$ ), demonstrating the superiority of FEMC with weakened solvating ability that helps to form more  $\text{Li}^+-\text{FSI}^-$  ion pairs.

In addition, the exact proportions of the solvent-separated ion pairs (i.e., SSIPs), one  $\text{FSI}^-$  anion coordinating to one  $\text{Li}^+$  (i.e.,

CIPs), and one  $\text{FSI}^-$  anion coordinating to two or more  $\text{Li}^+$  (i.e., AGGs) were also calculated according to MD simulations. As shown in Figure 2d, the FEMC-RCE is dominated by SSIPs (41%) and CIPs (58%), with little AGGs (1%). The AGGs were dramatically increased to 36% for FEMC-HCE, and further boosted to 39% for FEMC-LHCE. While only 12% AGGs were found for EMC-LHCE (Figure S2, Supporting Information), again demonstrating the merit of fluorinated FEMC solvent.

The coordination states of the solvent and anion in these electrolytes were further experimentally examined by Raman spectroscopy. The Raman band at  $710\text{--}770\text{ cm}^{-1}$  belongs to the S–N stretching vibration model,<sup>[31,32]</sup> which reflects the coordination state of the  $\text{FSI}^-$  anion. As shown in Figure 2e, the majority of the  $\text{FSI}^-$  anions present as SSIPs and CIPs in FEMC-RCE, while the peak position was significantly upshifted for both FEMC-HCE and FEMC-LHCE, indicating massive  $\text{FSI}^-$  anions turn to the state of CIPs and AGGs. Furthermore, as shown in Figure 2e, the free FEMC molecule shows an O–CH<sub>3</sub> stretching vibration band at  $907\text{ cm}^{-1}$ . In FEMC-RCE, the majority of the FEMC solvents exist in a free state because of high solvent-to-salt molar ratio (8.3, Table S1, Supporting Information). As the LiFSI concentration



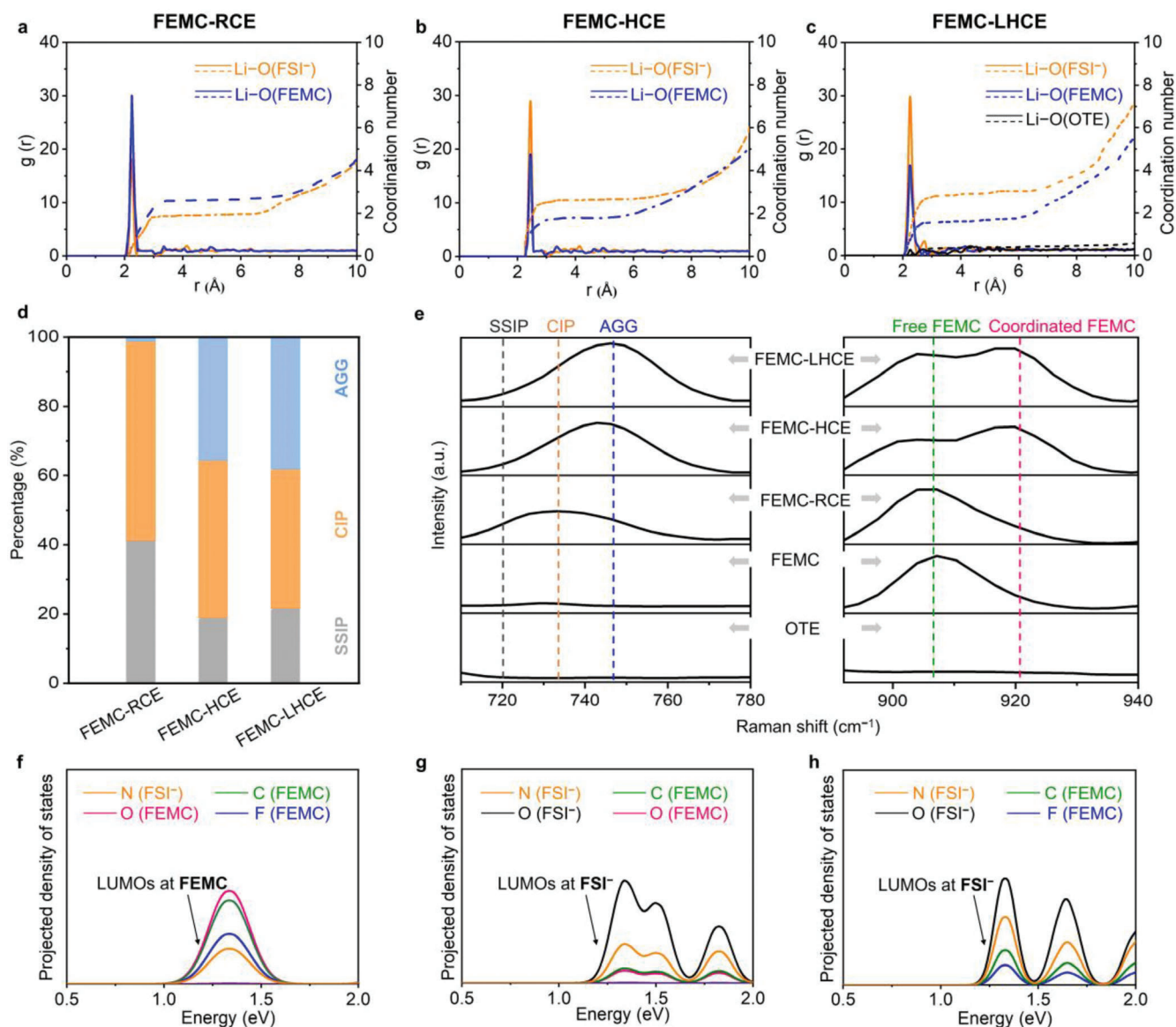


**Figure 2.** Theoretical and experimental studies of electrolyte solvation structures. The radial distribution functions calculated from MD simulations of a) FEMC-RCE, b) FEMC-HCE, and c) FEMC-LHCE. d) Distribution of the  $\text{Li}^+$  solvates in the FEMC-RCE, FEMC-HCE, and FEMC-LHCE systems. e) Raman spectra of the corresponding electrolytes and pure solvents. The PDOS calculated from DFT-MD simulations of f) FEMC-RCE, g) FEMC-HCE, and h) FEMC-LHCE.

increases, the solvent-to-salt molar ratio was decreased to 2.1 for both FEMC-HCE and FEMC-LHCE (Table S1, Supporting Information), resulting in a decreased proportion of free FEMC and increased proportion of  $\text{Li}^+$ -coordinated FEMC, as demonstrated by a new peak at  $922\text{ cm}^{-1}$ . Similar phenomenon was also observed for EMC-based electrolytes (Figure S4, Supporting Information).

The quantum mechanical density functional theory based molecular dynamics (DFT-MD) simulations was further carried out to elucidate the different reductive stability of the electrolytes, of which the projected density of states (PDOS) of equilibrium trajectories were shown in Figure 2f–h. The electrolyte component with the lowest LUMO energy will be reduced first to

form the inner SEI layer, followed by electrolyte component with higher LUMO energy to generate the outer SEI layer. The LUMO of the conduction band is located on the FEMC molecules in the FEMC-RCE system (Figure 2f), indicating that FEMC may be preferentially reduced to form a F-rich organic-dominated SEI layer. As shown in Figure 2g,h, the LUMOs of the conduction bands are transferred to  $\text{FSI}^-$  anions for both FEMC-HCE and FEMC-LHCE systems. Therefore,  $\text{FSI}^-$  anions, rather than FEMC solvents, may be preferentially reduced to form an inorganic SEI layer with high modulus. In addition, the fluorinated FEMC solvent with lower LUMO energy than that of EMC solvent is highly likely to be reduced following the reduction of  $\text{FSI}^-$  anions, contributing to a strong yet pliable F-rich organic outer layer

on the top of FSI<sup>−</sup>-derived inorganic inner layer, which builds a highly robust and stable F-rich inorganic–organic bilayer SEI.

The temperature-dependent viscosities and ionic conductivities are shown in Figures S5 and S6, Supporting Information. The FEMC-LHCE exhibits a much lower viscosity than that of FEMC-HCE at 25 °C (i.e., 13.39 vs 49.78 mPa s), leading to a much improved wettability as indicated by a small contact angle (i.e., 27.9°, Figure S7, Supporting Information). The FEMC-LHCE shows a lower ionic conductivity than that of FEMC-HCE (i.e., 0.6 vs 1.2 mS cm<sup>−1</sup>) even though it has low viscosity. This was ascribed to the intensified Li<sup>+</sup>–FSI<sup>−</sup> associations in FEMC-LHCE as well as the interruption of the Li<sup>+</sup>–ligand exchange by non-solvating OTE, which dismisses the fast Li<sup>+</sup> hopping conduction in FEMC-HCE as demonstrated by Dokko's recent study.<sup>[33]</sup> Nevertheless, its low ionic conductivity could be fully compensated by its much smaller SEI resistance ( $R_{\text{SEI}}$ ) and charge-transfer resistance ( $R_{\text{ct}}$ ), which would be demonstrated below.

## 2.2. Stable Cycling of SiMP Anodes

To verify the superiority of this electrolyte design strategy, the electrochemical performances of SiMP anode with a Si particle size of 1–5 μm was systematically investigated. As shown in Figure S8, Supporting Information, without any pretreatment, the Li||SiMP cell using FEMC-LHCE exhibits a high initial discharge capacity of 3360 mAh g<sup>−1</sup> (corresponding to ≈3.4 mAh cm<sup>−2</sup>) with a high initial CE of 89.1% at 0.1 C, which outperforms these using EMC-LHCE (3234 mAh g<sup>−1</sup>, 79.7%) and FEMC-RCE (3287 mAh g<sup>−1</sup>, 88.4%). Furthermore, as shown in Figure S9, Supporting Information, the capacity of the Li||SiMP cell using EMC-RCE drops rapidly to near 0 within ten cycles with highly fluctuated CE, indicating that the EMC-derived organic-dominated SEI is not stable to tolerate the volume change of the SiMP. In sharp contrast, the cell using FEMC-RCE exhibits a much improved cycling stability with a decent capacity retention of 26% after 100 cycles, which may be attributed to the strong yet pliable F-rich organic-dominated SEI derived by FEMC that bear the volume change of the SiMP to some extent, demonstrating the advantage of fluorinated FEMC over non-fluorinated EMC solvent.

Moreover, even with EMC-HCE or EMC-LHCE that is prone to generate an inorganic-dominated SEI with high modulus, the capacity of the cells still quickly decay to near 0 within 20 cycles, suggesting that such inorganic-dominated SEI can be rigid but is too fragile to sustain the vast volume change of the SiMPs upon cycling (Figure 3a and Figure S10, Supporting Information). In addition, further increasing the LiFSI concentration in EMC-LHCE system to 2.5 M (with a higher FSI<sup>−</sup>: solvent ratio of 1:1.9, Table S1, Supporting Information) do not improve the cycling performance of the cell (Figure S11, Supporting Information), indicating that solely rigid inorganic SEI is too fragile to sustain the vast volume change of the SiMPs upon cycling. Being markedly different from EMC-based electrolytes, the Li||SiMP cell using FEMC-LHCE presents stable cycling performance with a high capacity retention of 62% and a high average CE of ≈99.7% after 150 cycles at 0.2 C, and no obvious voltage polarization is observed in the charge–discharge curves during cycling (Figure 3d). This indicates that a much more robust and stable SEI than solely rigid

inorganic or flexible organic SEI was generated, which can effectively accommodate the immerse volume change of SiMPs.

For comparison purpose, the state-of-the-art commercial electrolytes with 5% FEC additive (denoted as CE+5%FEC), which has been reported to generate a mechanically stable LiF-containing organic–inorganic hybrid SEI,<sup>[18]</sup> was also subjected to the test. As shown in Figure 3a, the cell using CE+5%FEC can only retain 19% capacity over 150 cycles with a low average CE of 98.1% and large voltage polarization upon cycling (Figure 3b). Furthermore, the cycling performance of the Li||SiMP cell using FEMC-LHCE is also much better than the other non-fluorinated carbonate-based LHCE, namely, dimethyl carbonate (DMC)-LHCE that has recently been reported to enable the stable operable of Si/graphite anode<sup>[29]</sup> (<1000 mAh g<sup>−1</sup>). Unfortunately, the reported DMC-LHCE cannot sustain the stable cycling of Li||SiMP cell with only 24% capacity maintained with a low CE of 98.6% (Figure S12, Supporting Information), demonstrating the essential role of F-rich organic SEI components contributed from fluorinated solvent (i.e., FEMC). It should be noted that not all fluorinated solvents have such effect. For instance, the commonly used fluorinated solvent, FEC, is known to be able to generate a LiF-rich inorganic SEI components. However, the cell using FEC-LHCE displays a poor cycling with capacity drops to below 33% within 90 cycles with fluctuated CE (Figure S13, Supporting Information), indicating that solely F-rich inorganic SEI components is insufficient, which further illustrates the importance of this strong yet pliable F-rich organic SEI components in stabilizing SiMPs. In addition, the stable cycling of Li||SiMP cell at a higher rate of 0.4 C was also demonstrated in Figure S14, Supporting Information (80% capacity retained after 150 cycles).

The morphological evolution of the cycled SiMP anodes was first studied by scanning electron microscopy (SEM). As shown in Figure S15, Supporting Information, the pristine SiMP anode exhibits a thickness of 17.4 μm with micro-sized Si particles evenly distributed. However, after 50 cycles in CE+5%FEC, the thickness of the SiMP anode was dramatically increased to 43.8 μm, and severe cracks and pulverizations occurs (Figure 3e), leading to the loss of electrical connection and excessive growth of SEI, which accounts for fast capacity decay. Similar phenomenon was also observed for the SiMPs cycled in FEMC-RCE, indicating that the FEMC-derived organic-dominated SEI is still inadequate to tolerate the volume change of the SiMPs during cycling (Figure S16, Supporting Information). Since the SiMP anode can only survive for 20 cycles in EMC-LHCE, the SEM image was collected at 20th cycle. It seems like the expansion of the SiMP anode was mitigated in EMC-LHCE owing to the rigid inorganic SEI derived by anion, however, particle crack and disintegration were still found on the top view of the SiMP anode even after only 20 cycles (Figure 3f). In contrast, the SiMP anode cycled in FEMC-LHCE exhibits a lowest thickness of 22.6 μm and uniform morphology with no obvious cracks (Figure 3g), suggesting the effectiveness of SEI to withstand the volume change of the SiMPs.

Furthermore, the high-resolution transmission electron microscopy (TEM) image of the SiMP cycled in FEMC-LHCE also displays an intact particle morphology without any sign of mechanical fracture, and EDS mapping images show that the surface is covered with a thin SEI layer that is enriched with F, O, and S elements (Figure S17a, Supporting Information). While for the SiMP anode cycled in CE+5%FEC, internal pulverization

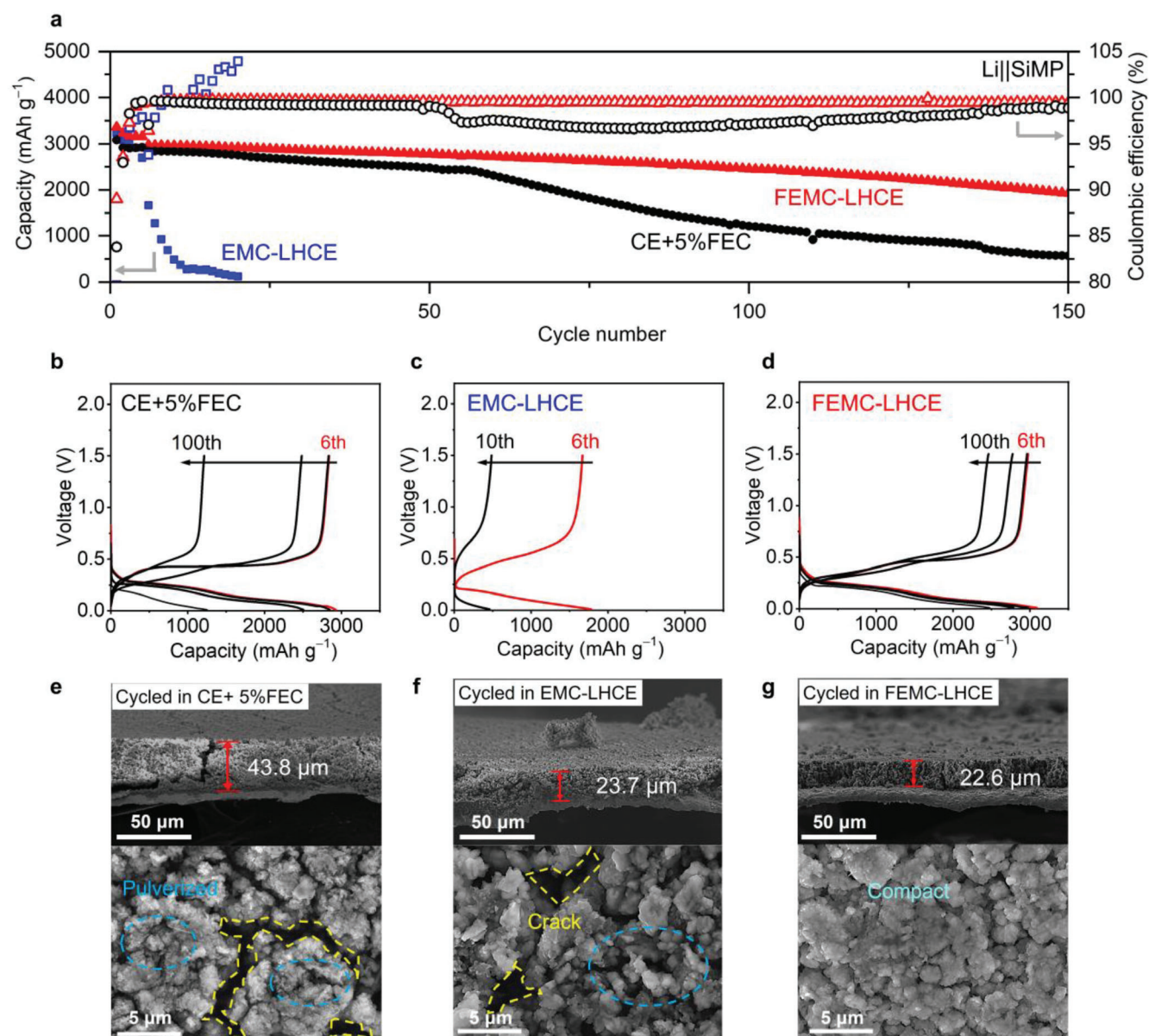


**Figure 3.** Electrochemical performance of Li||SiMP half-cells. a) Long-term cycling performance of the SiMP anodes in CE+5%FEC, EMC-LHCE, and FEMC-LHCE at 0.2 C after five formation cycles at 0.1 C. Selected charge–discharge curves of the Li||SiMP cells using b) CE+5%FEC, c) EMC-LHCE, and d) FEMC-LHCE. Cross-sectional and top-view SEM images of the SiMP electrodes in e) CE+5%FEC after 50 cycles, f) EMC-LHCE after 20 cycles, and g) FEMC-LHCE after 50 cycles.

can be found, along with a thick and non-uniform layer that is enriched with F, O, and P elements covered on the Si particle surface (Figure S17b, Supporting Information), suggesting over decomposition of the electrolyte due to its unstable interphase.

### 2.3. F-Rich Inorganic–Organic Bilayer SEI

The dramatically different electrochemical behaviors of the SiMPs in different electrolytes are mainly originated from their different SEI chemistry, which was analyzed by X-ray photoelectron spectroscopy (XPS) with an Ar<sup>+</sup> sputtering depth profiling.

The SiMP anodes used for XPS measurement were recovered from the Li||SiMP half-cells after 50 cycles, except for that using EMC-LHCE since the cell failed after 20 cycles. For the SiMP anode cycled in FEMC-RCE electrolyte (Figure 4a), the surface of the SEI is enriched with organic species of –CF<sub>3</sub> and RCO<sub>2</sub>Li derived from FEMC solvent, of which the intensities remain almost unchanged as the Ar<sup>+</sup> sputtering time increases. Meanwhile, some inorganic species of LiF, oxysulfides, and oxynitrides derived from FSI<sup>−</sup> anion were also identified, while their intensities slightly reduced as the Ar<sup>+</sup> sputtering time increases. Time-of-flight secondary ion mass spectroscopy (TOF-SIMS) was further employed to reveal the distribution of these species in the



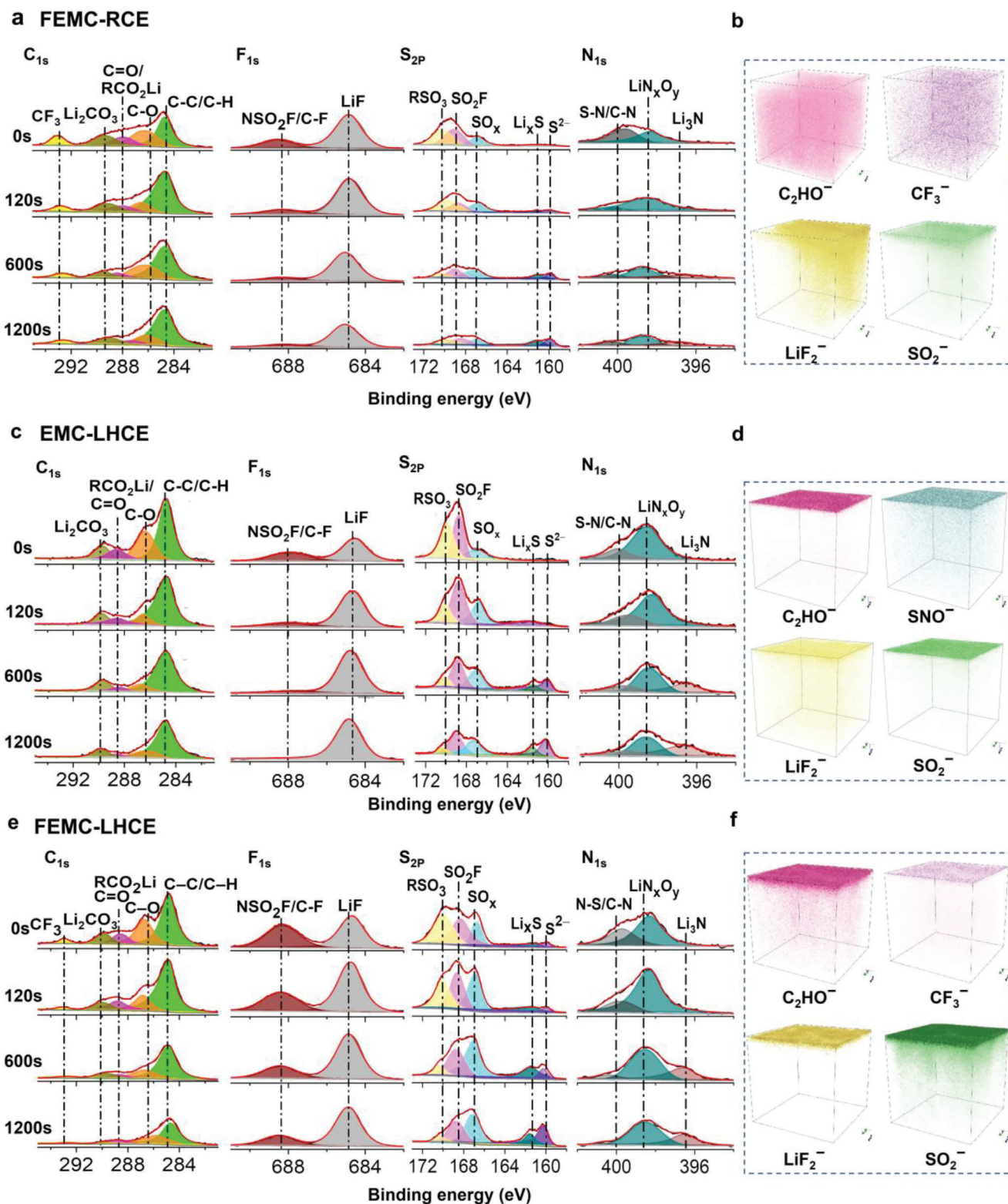


**Figure 4.** SEI chemical composition and distribution. XPS spectra of the cycled SiMP anode using a) FEMC-RCE, c) EMC-LHCE, and e) FEMC-LHCE. The  $C_{1s}$ ,  $F_{1s}$ ,  $S_{2p}$ , and  $N_{1s}$  spectra are displayed in columns, which show the corresponding depth profiling results. 3D TOF-SIMS sputtering images of selected secondary ion fragments of  $C_2HO^-$ ,  $CF_3^-$ ,  $LiF_2^-$ ,  $SO_2^-$  and  $SNO^-$  on cycled SiMP using b) FEMC-RCE, d) EMC-LHCE, and f) FEMC-LHCE.

SEI. As shown in Figure 4b, the 3D reconstructed sputtering images show that the organic fragments  $C_2HO^-$  and  $CF_3^-$  are uniformly distributed, while the inorganic fragments  $LiF_2^-$  and  $SO_2^-$  has less concentration aggregation, suggesting that the SEI derived in FEMC-RCE is mainly consisted of  $CF_3$ -rich organic-dominated species with an improved interfacial energy compared to that of pure organic SEI (Figure 5a), which can support the lithiation/delithiation of SiMPs to certain extent (Figure S9, Supporting Information), but still insufficient to sustain the immense volume change of the SiMP during repeated cycling.

For the SiMPs cycled in EMC-LHCE, the surface of the SEI consists of both organic ( $RCO_2Li$ ) and inorganic species ( $LiF$ , oxysulfides, and oxynitrides). As the  $Ar^+$  sputtering proceeds, the content of organic species decreases significantly, while inorganic  $LiF$  content increases continuously with a new  $Li_3N$  peak appears (Figure 4c). Together with the TOF-SIMS sputtering images shown in Figure 4d, it can be concluded that the SEI derived in EMC-LHCE is mainly composed of inorganic components with a small amount of organic components on the surface. As schematically shown in Figure 5b, such inorganic-dominated SEI is too rigid to tolerate the vast volume change of SiMP, resulting in disintegration of the SiMP and rapid capacity decay (Figure 3c,f).

For the SiMP cycled in FEMC-LHCE, the surface of the SEI is enriched with organic species of  $-CF_3$  and  $RCO_2Li$  derived from FEMC solvent, of which their intensities dramatically reduced to less than 10% after 120 s of  $Ar^+$  sputtering (Figure 4e), indicating that such F-rich organic components are only existed on the top surface of the SEI. In contrast, the content of  $LiF$  keeps rising with the increasing  $Ar^+$  sputtering time, and the contents of other inorganic species, such as oxysulfides, oxynitrides, and  $Li_3N$ , remain relatively high even after 1200 s of  $Ar^+$  sputtering time, suggesting that the inner of the SEI is high-purity F-rich inorganic components (Figure 4f). This results in a highly robust and stable F-rich inorganic–organic bilayer SEI (Figure 5c), of which the high-modulus F-rich inorganic inner layer plays a role in accommodating the plastic deformation of SiMP, and the dense, strong yet pliable F-rich organic outer layer acts as a buffer layer to alleviating the stress from inorganic inner layer as well as to prevent parasitic reaction with electrolytes, thereby enabling the stable cycling of SiMP anode with high CE (Figure 3).

For comparison purpose, the SiMP anode cycled in CE+5%FEC was also investigated. As shown in Figures S18 and S19, Supporting Information, a  $LiF$ -containing inorganic–organic hybrid SEI was detected on the surface of SiMP anode. The inner organic components may increase the adhesion of SEI to the lithiated Si, which leads to SEI deformation and rupture during cycling,<sup>[25]</sup> resulting in an unsatisfactory cycling performance with low CE (Figure 3).

The lithiation of the SiMP anode involves not only the transport of solvated  $Li^+$  in the bulk electrolyte but also the desolvation of solvated  $Li^+$  and subsequent migration of  $Li^+$  through SEI, which was investigated by electrochemical impedance spectra (EIS). As shown in Figure S20, Supporting Information, even though the cell using FEMC-LHCE exhibits a relatively large electrolyte bulk resistance ( $R_e$ ) due to its low ionic conductivity, however, it could be fully compensated by much lower SEI and desolvation resistance ( $R_{SEI} + R_{dsv}$ ). Furthermore, the resistance remains quick stable even after 100 cycles for the cell using FEMC-

LHCE (Figure S20c, Supporting Information), while the resistance increases dramatically for that using FEMC-RCE, EMC-LHCE, or CE+5%FEC, which was mainly attributed to the thin, robust, and stable F-rich inorganic–organic bilayer SEI derived by FEMC-LHCE.

## 2.4. Stable Operation of High-Energy-Density SiMP||NMC811 and SiMP||LNMO Full-Cells

To maximize the energy density of LiBs, in addition to using high-capacity SiMP anode, high-capacity/high-voltage cathodes should be employed (e.g., NMC811 and LNMO). Therefore, the anodic stability of the electrolyte was first examined. The intrinsic oxidation stability of the electrolyte was first evaluated by linear sweep voltammetry (LSV) with a platinum (Pt) plate as working electrode. As shown in the Figure 6a, both CE+5%FEC and EMC-LHCE show an oxidation stability of  $\approx 4.4$  V, which is significantly improved to above 5.0 V for the FEMC-LHCE, owing to the electron-withdrawing fluorine moiety that lowers the HOMO of the FEMC solvent thermodynamically.<sup>[34,35]</sup> When testing on an Al working electrode, it was found that the current rises at  $\approx 4.0$  V in EMC-LHCE because of the anodic corrosion of Al electrode, whereas the potential is largely postponed to beyond 5.2 V for FEMC-LHCE (Figure S21, Supporting Information), demonstrating its effectiveness in inhibiting Al corrosion. The chronoamperometry (CA) test of  $Li||Al$  cell was further carried out to show the superiority of the FEMC-LHCE (Figure 6b). After holding at 4.9 V for 24 h, high leakage current ( $23 \mu A cm^{-2}$ ) and severe corrosion spots on Al is observed for the cell using EMC-LHCE, indicating severe Al corrosion and electrolyte decomposition. In sharp contrast, negligible leakage current ( $0.14 \mu A cm^{-2}$ ) and no Al corrosion is found for FEMC-LHCE, which is attributed to the following three merits: 1) the unique solvation structure of the FEMC-LHCE that has little free FEMC solvent to dissolve  $Al^{3+}$  complexes, 2) besides, the solvating ability of the FEMC was weakened by its electron-withdrawing fluorine moiety, making the electrolyte show low solvating power to diffuse  $Al^{3+}$  complexes, and 3) moreover, the fluorine moiety also lowers the HOMO of solvent that dramatically improve the oxidation stability of the electrolyte.

Having confirmed the superiority of the F-rich inorganic–organic SEI in stabilizing SiMP anode as well as the high anodic stability, the rational designed FEMC-LHCE was also further investigated as a promising electrolyte in the high-voltage high-energy-density SiMP||NMC811 ( $\approx 3.0$  mAh  $cm^{-2}$ ) and SiMP||LNMO ( $\approx 1.7$  mAh  $cm^{-2}$ ) full-cells. It should be noted that no prelithiation or precycling was conducted on SiMP anode. As shown in Figure 6d and Figure S22, Supporting Information, under a high cutoff voltage of 4.3 V, for the SiMP||NMC811 cell using CE+5%FEC, the capacity quickly drops to less than 15% within 100 cycles, whereas much improved cycling performance is achieved for the cell using FEMC-LHCE. To ensure the structural integrity of the cathode under high-voltage, a small amount of FEC additive (2%, by vol.) was added to FEMC-LHCE (denoted as FEMC-LHCE+2%FEC) to construct a stable  $LiF$  cathode–electrolyte interphase.<sup>[36]</sup> As shown in Figure S23, Supporting Information, the cell using FEMC-LHCE+2%FEC delivers a high initial capacity of 195 mAh  $g^{-1}$  with a high average



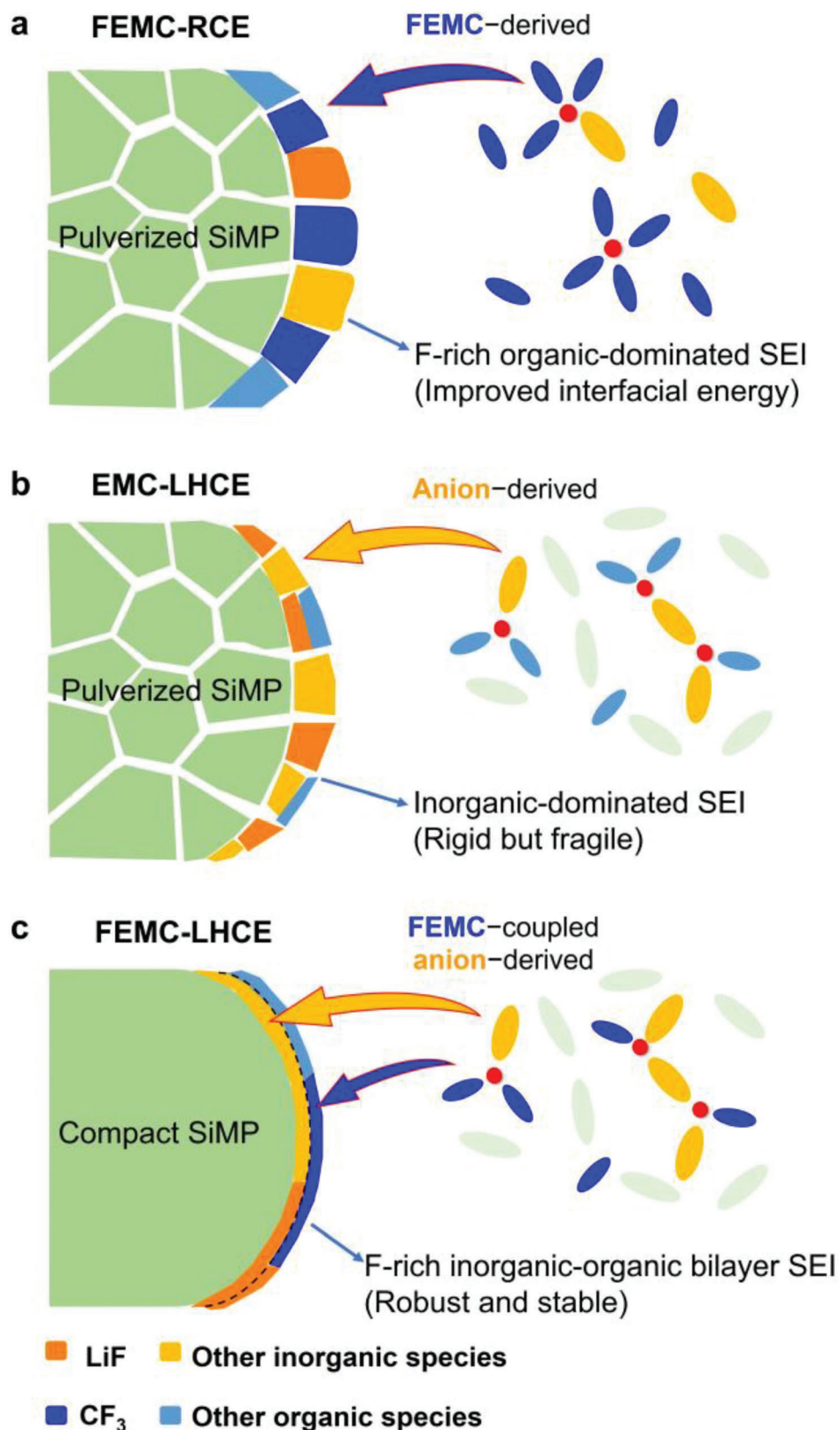


**Figure 5.** The influence of electrolyte solvation chemistry on SEI. Schematic illustration of the SEI on the SiMP anode cycled in a) FEMC-RCE, b) EMC-LHCE, and c) FEMC-LHCE.

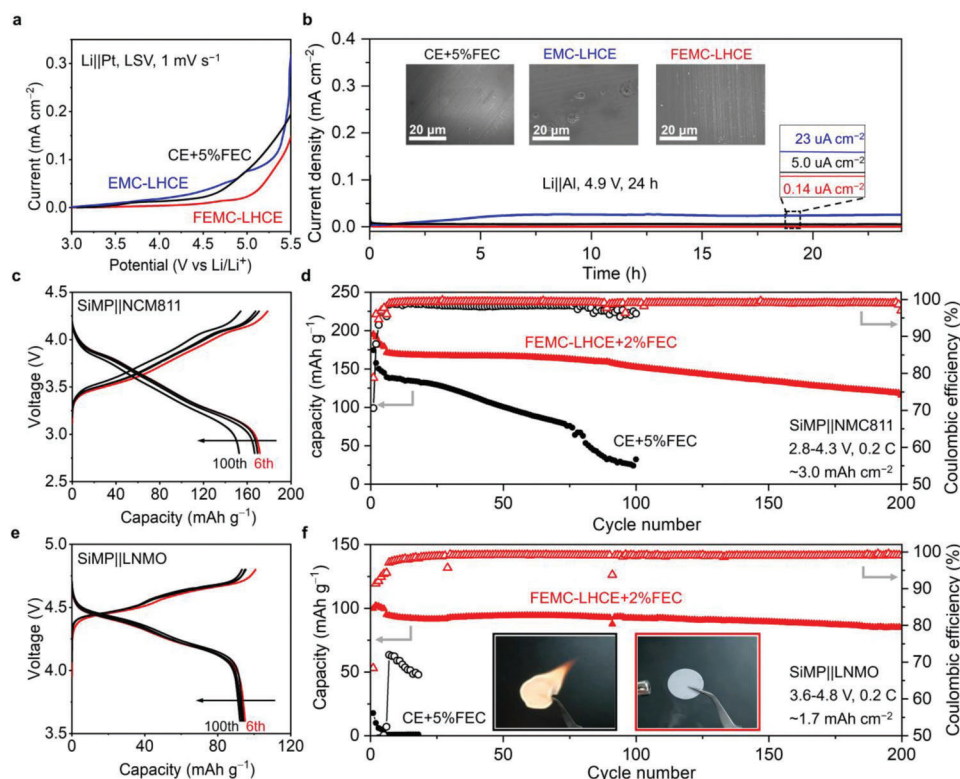


**Figure 6.** Electrochemical performance of SiMP||NMC811 and SiMP||LNMO coin-cells. a) The linear scan voltammetry (LSV) of the electrolytes with Pt as working electrode in a three-electrode cell at a scan rate of  $1 \text{ mV s}^{-1}$ . b) Chronoamperometry (CA) profiles of Li||Al cells in different electrolytes at 4.9 V versus Li/Li<sup>+</sup> for 24 h. The insets show SEM images of Al electrodes after CA tests. Selected charge-discharge curves of c) SiMP||NMC811 and e) SiMP||LNMO cells in FEMC-LHCE+2%FEC. Long-term cycling performance of d) SiMP||NMC811 and f) SiMP||LNMO cells in different electrolytes at 0.2 C after five formation cycles at 0.1 C. The insets show the flammability tests of the FEMC-LHCE and CE+5%FEC electrolyte.

operating voltage of 3.5 V, corresponding to an extremely high energy density of  $\approx 640 \text{ Wh kg}^{-1}$  based on the total active masses of the cathode and anode, which is among the highest energy density reported thus far for LiBs. The SiMP||NMC811 cell also demonstrates excellent cycling stability with a high capacity retention of 70% and a high CE of 99.8% after 200 cycles at 0.2 C. Furthermore, even under such high areal loading of  $\approx 3.0 \text{ mAh cm}^{-2}$ , no obvious voltage polarization is observed (Figure 6c). Furthermore, the SiMP||NMC811 cell using FEMC-LHCE+2%FEC is also proven to operate stably at a high temperature of  $55^\circ\text{C}$ , while the capacity quickly drops to near 0 for that using CE+5%FEC (Figure S24, Supporting Information). After 100 cycles, obvious cracking of the NMC811 cathode particle was observed that results in the loss of electrical connection and fast capacity decay, while the microstructure of NMC811 cathode using FEMC-LHCE+2%FEC remains intact with negligible change (Figure S25, Supporting Information). Moreover, as shown in Figure S26, Supporting Information, the concentration of dissolved Ni in FEMC-LHCE+2%FEC is only 1/20 of that in the CE+5%FEC after cycling, which clearly demonstrates that the designed FEMC-LHCE+2%FEC can effectively protect the cathode.

Remarkably, the FEMC-LHCE+2%FEC also enables the stable operation of the full-cell with a 5 V-class LNMO cathode. As shown in Figure S27, Supporting Information, under a high cutoff voltage of 4.8 V, the SiMP||LNMO cell delivers an initial capacity of  $100 \text{ mAh g}^{-1}$  with a high average operating voltage

of 4.3 V. Furthermore, the cell exhibits extremely stable cycling performance with more than 90% capacity retained after 200 cycles (Figure 6f), and no increase in voltage polarization can be observed (Figure 6e). In sharp contrast, due to its inferior SEI on SiMP anode side and insufficient oxidation stability of the electrolyte under high-voltage, the SiMP||LNMO cell using CE+5%FEC cannot operate normally, with the capacity rapidly drops to near 0 within ten cycles (Figure 6f and Figure S28, Supporting Information). Moreover, compared with the highly flammable commercial electrolyte, the rational designed FEMC-LHCE electrolyte is completely nonflammable (Movies S1 and S2, Supporting Information), ensuring the safety of high-energy-density batteries.

The superiority of the FEMC-LHCE electrolyte was eventually subjected to the test of practical pouch cell. As shown in Figure 7a, a 1.0 Ah SiMP||NMC811 pouch-cell with an eight-layer assembly using FEMC-LHCE+2%FEC demonstrates excellent cycling stability with more than 62% capacity maintained and a high CE of 99.8% after 200 cycles at 0.2 C, which is the best cycling performance ever achieved for Ah-level pouch-cell using high capacity micro-sized Si anode of  $\geq 1500 \text{ mAh g}^{-1}$  under high cut-off voltage of  $\geq 4.1 \text{ V}$  (Figure 7c and Table S2, Supporting Information). Actually, we have searched the literatures carefully and found only one paper reported a 1.2 Ah pouch-cell using a carbon-encapsulated SiMP, however, only 30 cycles was shown and a costly prelithiation step is adopted.<sup>[10]</sup> Moreover, for

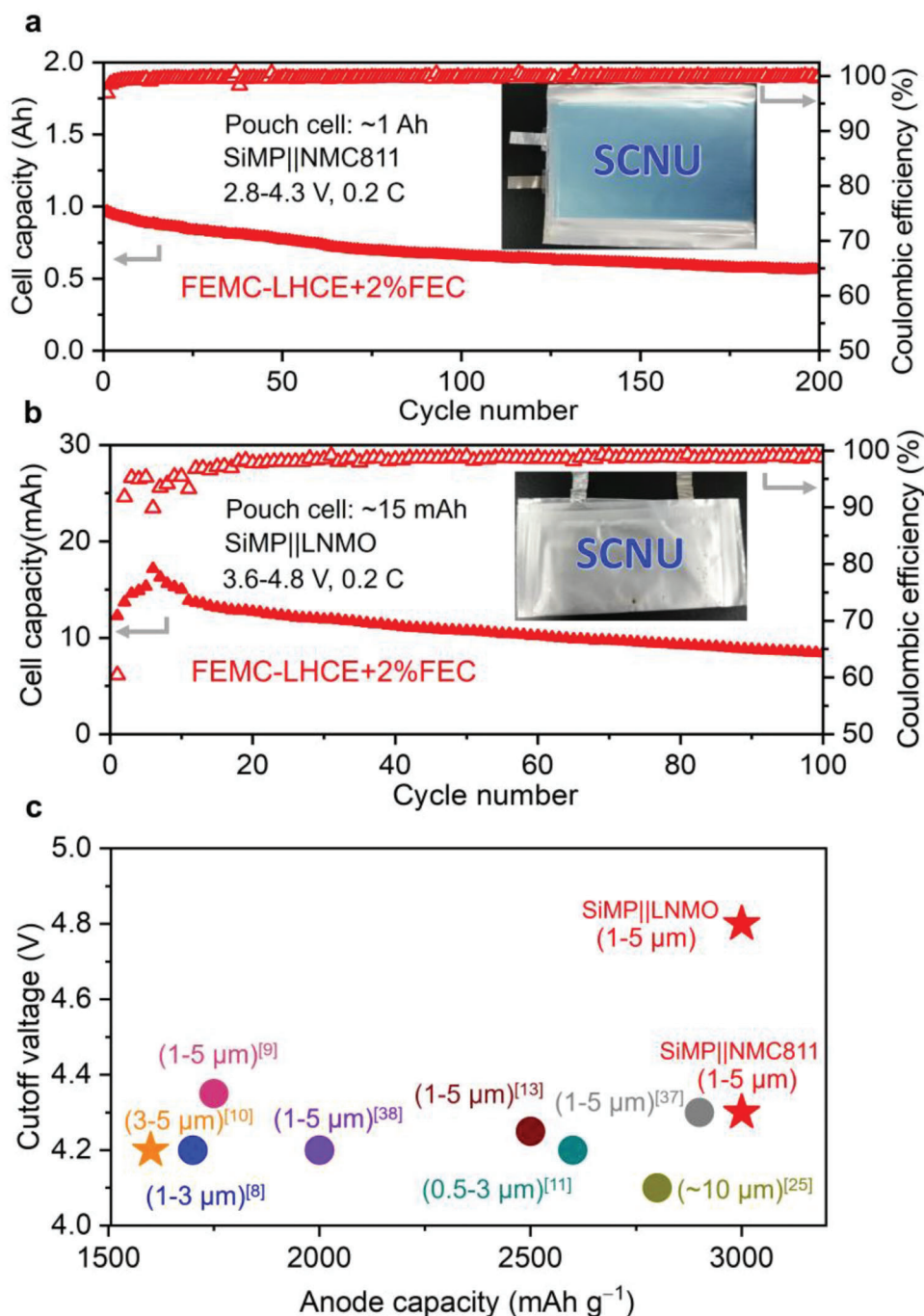


**Figure 7.** Electrochemical performance of SiMP||NMC811 and SiMP||LNMO pouch-cells. a) Cycling performance of a 1.0 Ah SiMP||NMC811 pouch-cell using FEMC-LHCE+2%FEC at 0.2 C after five cycles at 0.1 C. b) Cycling performance of a 15 mAh SiMP||LNMO pouch-cell using FEMC-LHCE+2%FEC at 0.2 C after five cycles at 0.1 C. c) Comparison of the full-cell containing SiMP anode with other reported work (SiMP||NCA,<sup>[25]</sup> SiMP@Gr||LCO,<sup>[8]</sup> SiMP||NMC811,<sup>[10]</sup> SiMP||sulfide||NMC811,<sup>[37]</sup> PAA-P(HEA-co-DMA)-SiMP||NMC111,<sup>[11]</sup> PR-PAA-SiMP||NCA,<sup>[13]</sup> mSi@OG@RGO||LCO,<sup>[9]</sup> and SiMP||sulfide||NCA<sup>[38]</sup>) in terms of anode capacity ( $\geq 1500 \text{ mAh g}^{-1}$ ), silicon size ( $\geq 1 \mu\text{m}$ ), and upper cutoff voltage ( $\geq 4.1 \text{ V}$ ). The star mark indicates both coin-cell and pouch-cell was studied, while circular mark means only coin-cell was studied.

the first time, a single layer SiMP||LNMO pouch-cell with high capacity SiMP anode under high cut-off voltage of 4.8 V was demonstrated (Figure 7b). The pouch-cell using FEMC-LHCE+2%FEC delivers a very decent cycling stability with more than 63% capacity maintained after 100 cycles.

### 3. Conclusions

In summary, we herein rationally design a fluorinated solvent (i.e., FEMC)-based LHCE for high-energy-density LiBs to overcome the longstanding challenges of structural pulverization of



SiMP anode and high-voltage cathode incompatibility. The combined theoretical and experimental studies have demonstrated that the fluorine moiety lowers the solvating power of FEMC that promotes  $\text{Li}^+$ -FSI $^-$  pairing, which leads to a high-modulus LiF-rich inorganic inner SEI layer to accommodate the plastic deformation of SiMP. Furthermore, the subsequent reduction of FEMC solvent contributes to a dense, strong yet pliable  $\text{CF}_3$ -rich organic outer SEI layer, which not only acts as a buffer layer to alleviate the stress from inorganic inner layer but also prevents parasitic reaction with electrolytes. This yields a highly robust and stable F-rich inorganic-organic bilayer SEI to enable stable cycling of pristine SiMP anode (without any treatment) with an ultrahigh CE of 99.7%. Coupled with its high anodic stability, the FEMC-LHCE also endows the stable operation of high-energy-density SiMP||NMC811 ( $640 \text{ Wh kg}^{-1}$ ) and SiMP||LNMO ( $408 \text{ Wh kg}^{-1}$ ) coin- and pouch-cells (Ah level), which represents one of the best performance for the full-cell using high capacity micro-sized Si anodes and high-voltage cathodes. Therefore, this work demonstrates the effectiveness of incorporating fluorinated solvent into LHCE as well as offers fundamental understanding of fluorinated solvent-coupled anion-derived interfacial chemistry in stabilizing SiMP, which provides a simple yet efficient electrolyte design strategy toward the practical application of high-energy-density LIBs with high capacity SiMP anodes.

## 4. Experimental Section

**Materials Characterization:** The Raman spectra of the electrolyte solutions were collected using a QE65 Pro spectrometer (Ocean Optics) with a laser excitation wavelength of 532 nm. The density and viscosity of electrolytes were determined by SVM3001 (Anton Paar) with the temperature range from  $-20$  to  $40^\circ\text{C}$ . The wettability test was carried out on a contact angle measuring equipment (JC2000D3P, POWEREACH). The surface chemical compositions of the electrodes were analyzed using XPS (PerkinElmer PHI 1600 ESCA). The morphologies of the electrodes were investigated using a SEM (MAIA3, TESCAN Brno, s.r.o.) and TEM (JEM-2100 HR). The cells were disassembled in an Ar-filled glovebox, rinsed three times with its corresponding solvent, and then dried under vacuum, and thus it was assumed that no residual salt or solvent remained on the surface of the electrodes. For XPS measurement, the washed electrodes were transferred from the glovebox to the XPS chamber without exposure to air. The TOF-SIMS characterization of the cycled SiMP anodes was performed at the Suzhou Institute of Nano-Tech, and Nano-Bionics, Chinese Academy of Sciences. The contents of the dissolved transition metal ions were measured using an inductively coupled plasma optical emission spectrometry (SPECTRO ARCOS MV).

**Electrochemical Measurements:** Using an Ar-filled glovebox, Li||SiMP, SiMP||NMC811, and SiMP||LNMO cells were assembled in a standard 2032-type coin-cell with Celgard 3501 and glass fiber (Advantec GC-50) as separator. The electrolyte amount for each cell was  $80 \mu\text{L}$ . An eight-layer SiMP||NMC811 pouch cell with a capacity of  $\approx 1 \text{ Ah}$  and a single-layer SiMP||LNMO pouch cell with a capacity of  $\approx 15 \text{ mAh}$  was also assembled with a Celgard 3501 as separator in the glovebox. The galvanostatic charge-discharge tests of both coin- and pouch-cells were conducted using a LAND CT2001A instrument (Wuhan Jinnuo Electronic Co. Ltd.) at different rate. A symmetrical Pt|electrolyte|Pt cell was used to measure the ionic conductivity of the electrolytes via EIS method. The EIS spectra were collected at the temperature ranging from  $-20$  to  $40^\circ\text{C}$  with an amplitude of  $10 \text{ mV}$  within the frequency ranging from  $10^6$  to  $0.1 \text{ Hz}$ . The anodic stability of the electrolytes was investigated by LSV on a three-electrode configuration using Pt plate or Al foil as working electrode and lithium metal as both reference and counter electrodes at a scan rate of  $1 \text{ mV s}^{-1}$  from the open circuit voltage to  $6.5 \text{ V}$  at  $25^\circ\text{C}$ . The chronoamperometry

(CA) test was conducted by holding Li||Al cell at  $4.9 \text{ V}$  for  $24 \text{ h}$ . The EIS, LSV, and CA were measured using a Potentiostat (VMP3, Bio-Logic).

**Statistical Analysis:** All results were performed with the sample size of  $n \geq 3$ . No further adjustments were made to the data before statistical analysis. The statistics were expressed as the mean values  $\pm$  SD (standard deviation). Origin 2019 was used for analysis.

## Supporting Information

Supporting Information is available from the Wiley Online Library or from the author.

## Acknowledgements

Y.L., Y.H., and X.X. contributed equally to this work. This work was supported by the National Natural Science Foundation of China (No. 22005108), the Natural Science Foundation of Guangdong Province (No. 2022B1515020005), and the Department of Science and Technology of Guangdong Province (Nos. 2021A0505030063 and 2020B0101030005).

## Conflict of Interest

The authors declare no conflict of interest.

## Data Availability Statement

The data that support the findings of this study are available from the corresponding author upon reasonable request.

## Keywords

bilayer solid-electrolyte interphase, fluorinated solvents, high-energy-density batteries, localized high-concentration electrolytes, Si microparticle anodes

Received: April 2, 2023

Revised: April 26, 2023

Published online:

- [1] S. Chae, M. Ko, K. Kim, K. Ahn, J. Cho, *Joule* **2017**, 1, 47.
- [2] S. Goriparti, E. Miele, F. De Angelis, E. Di Fabrizio, R. Proietti Zaccaria, C. Capiglia, *J. Power Sources* **2014**, 257, 421.
- [3] Y. Jin, B. Zhu, Z. Lu, N. Liu, J. Zhu, *Adv. Energy Mater.* **2017**, 7, 1700715.
- [4] W. Liu, P. Oh, X. Liu, M. J. Lee, W. Cho, S. Chae, Y. Kim, J. Cho, *Angew. Chem., Int. Ed.* **2015**, 54, 4440.
- [5] Y. Sun, N. Liu, Y. Cui, *Nat. Energy* **2016**, 1, 16017.
- [6] G. Zhu, D. Chao, W. Xu, M. Wu, H. Zhang, *ACS Nano* **2021**, 15, 15567.
- [7] J. D. McBrayer, M.-T. F. Rodrigues, M. C. Schulze, D. P. Abraham, C. A. Appleby, I. Bloom, G. M. Carroll, A. M. Colclasure, C. Fang, K. L. Harrison, G. Liu, S. D. Minter, N. R. Neale, G. M. Veith, C. S. Johnson, J. T. Vaughey, A. K. Burrell, B. Cunningham, *Nat. Energy* **2021**, 6, 866.
- [8] Y. Li, K. Yan, H.-W. Lee, Z. Lu, N. Liu, Y. Cui, *Nat. Energy* **2016**, 1, 15029.
- [9] X. Zhang, R. Guo, X. Li, L. Zhi, *Small* **2018**, 14, 1800752.
- [10] F. Chen, J. Han, D. Kong, Y. Yuan, J. Xiao, S. Wu, D. M. Tang, Y. Deng, W. Lv, J. Lu, F. Kang, Q. H. Yang, *Kwansei Gakuin Univ. Nat. Sci. Rev.* **2021**, 8, nwab012.

- [11] Z. Xu, J. Yang, T. Zhang, Y. Nuli, J. Wang, S.-i. Hirano, *Joule* **2018**, 2, 950.
- [12] C. Wang, H. Wu, Z. Chen, M. T. McDowell, Y. Cui, Z. Bao, *Nat. Chem.* **2013**, 5, 1042.
- [13] S. Choi, T.-w. Kwon, A. Coskun, J. W. Choi, *Science* **2017**, 357, 279.
- [14] W. An, B. Gao, S. Mei, B. Xiang, J. Fu, L. Wang, Q. Zhang, P. K. Chu, K. Huo, *Nat. Commun.* **2019**, 10, 1447.
- [15] S. Yang, Y. Zhang, Z. Li, N. Takenaka, Y. Liu, H. Zou, W. Chen, M. Du, X.-J. Hong, R. Shang, E. Nakamura, Y.-P. Cai, Y.-Q. Lan, Q. Zheng, Y. Yamada, A. Yamada, *ACS Energy Lett.* **2021**, 6, 1811.
- [16] Y. Zhang, N. Du, D. Yang, *Nanoscale* **2019**, 11, 19086.
- [17] K. Kim, H. Ma, S. Park, N.-S. Choi, *ACS Energy Lett.* **2020**, 5, 1537.
- [18] C. Xu, F. Lindgren, B. Philippe, M. Gorgoi, F. Björefors, K. Edström, T. Gustafsson, *Chem. Mater.* **2015**, 27, 2591.
- [19] Z. Hu, L. Zhao, T. Jiang, J. Liu, A. Rashid, P. Sun, G. Wang, C. Yan, L. Zhang, *Adv. Funct. Mater.* **2019**, 29, 1906548.
- [20] G.-B. Han, J.-N. Lee, J. W. Choi, J.-K. Park, *Electrochim. Acta* **2011**, 56, 8997.
- [21] S. J. Lee, J.-G. Han, Y. Lee, M.-H. Jeong, W. C. Shin, M. Ue, N.-S. Choi, *Electrochim. Acta* **2014**, 137, 1.
- [22] S. Park, S. Y. Jeong, T. K. Lee, M. W. Park, H. Y. Lim, J. Sung, J. Cho, S. K. Kwak, S. Y. Hong, N. S. Choi, *Nat. Commun.* **2021**, 12, 838.
- [23] T. Jaumann, J. Balach, U. Langklotz, V. Sauchuk, M. Fritsch, A. Michaelis, V. Teltevskij, D. Mikhailova, S. Oswald, M. Klose, G. Stephani, R. Hauser, J. Eckert, L. Giebeler, *Energy Storage Mater.* **2017**, 6, 26.
- [24] Y. Yamada, J. Wang, S. Ko, E. Watanabe, A. Yamada, *Nat. Energy* **2019**, 4, 269.
- [25] J. Chen, X. Fan, Q. Li, H. Yang, M. R. Khoshi, Y. Xu, S. Hwang, L. Chen, X. Ji, C. Yang, H. He, C. Wang, E. Garfunkel, D. Su, O. Borodin, C. Wang, *Nat. Energy* **2020**, 5, 386.
- [26] S. Chen, J. Zheng, D. Mei, K. S. Han, M. H. Engelhard, W. Zhao, W. Xu, J. Liu, J. G. Zhang, *Adv. Mater.* **2018**, 30, 1706102.
- [27] S. Chen, J. Zheng, L. Yu, X. Ren, M. H. Engelhard, C. Niu, H. Lee, W. Xu, J. Xiao, J. Liu, J.-G. Zhang, *Joule* **2018**, 2, 1548.
- [28] H. Jia, L. Zou, P. Gao, X. Cao, W. Zhao, Y. He, M. H. Engelhard, S. D. Burton, H. Wang, X. Ren, Q. Li, R. Yi, X. Zhang, C. Wang, Z. Xu, X. Li, J. G. Zhang, W. Xu, *Adv. Energy Mater.* **2019**, 9, 1900784.
- [29] S. Chae, W.-J. Kwak, K. S. Han, S. Li, M. H. Engelhard, J. Hu, C. Wang, X. Li, J.-G. Zhang, *ACS Energy Lett.* **2021**, 6, 387.
- [30] Z. Cao, X. Zheng, Q. Qu, Y. Huang, H. Zheng, *Adv. Mater.* **2021**, 33, 2103178.
- [31] K. Ding, C. Xu, Z. Peng, X. Long, J. Shi, Z. Li, Y. Zhang, J. Lai, L. Chen, Y. P. Cai, Q. Zheng, *ACS Appl. Mater. Interfaces* **2022**, 14, 44470.
- [32] J. Shi, C. Xu, J. Lai, Z. Li, Y. Zhang, Y. Liu, K. Ding, Y. P. Cai, R. Shang, Q. Zheng, *Angew. Chem., Int. Ed.* **2023**, 62, e202218151.
- [33] Y. Watanabe, Y. Ugata, K. Ueno, M. Watanabe, K. Dokko, *Phys. Chem. Chem. Phys.* **2023**, 25, 3092.
- [34] X. Fan, L. Chen, O. Borodin, X. Ji, J. Chen, S. Hou, T. Deng, J. Zheng, C. Yang, S. C. Liou, K. Amine, K. Xu, C. Wang, *Nat. Nanotechnol.* **2018**, 13, 715.
- [35] Q. Zheng, Y. Yamada, R. Shang, S. Ko, Y.-Y. Lee, K. Kim, E. Nakamura, A. Yamada, *Nat. Energy* **2020**, 5, 291.
- [36] Y. Xu, J. Liu, L. Zhou, L. Zeng, Z. Yang, *J. Electroanal. Chem.* **2017**, 791, 109.
- [37] D. H. S. Tan, Y. T. Chen, H. Yang, W. Bao, B. Sreenarayanan, J. M. Doux, W. Li, B. Lu, S. Y. Ham, B. Sayahpour, J. Scharf, E. A. Wu, G. Deysher, H. E. Han, H. J. Hah, H. Jeong, J. B. Lee, Z. Chen, Y. S. Meng, *Science* **2021**, 373, 1494.
- [38] Y. Huang, B. Shao, Y. Wang, F. Han, *Energy Environ. Sci.* **2023**, 16, 1569.